Int. J. Plasma Environ. Sci. Technol. 16 (2022) e03005 (9pp)

International Journal of Plasma Environmental Science and Technology

Regular Paper

DOI: 10.34343/ijpest.2022.16.e03005

Local temperature control device using a transparent electrode in the viewing area of a microscope: development and application to RT-PCR

Masahiko Oshige[1, 2], Ryo Yokosawa[1], Hitomi Shinohara[1], Maho Suzuki[1], Shinji Katsura[1, 2,*]

[1] Department of Environmental Engineering Science,
Graduate School of Science and Technology, Gunma University, Japan
[2] Gunma University Center for Food Science and Wellness (GUCFW), Japan

* Corresponding author: katsura@gunma-u.ac.jp (Shinji Katsura)

Received: 22 September 2022
Revised: 16 November 2022
Accepted: 16 November 2022
Published online: 22 November 2022

Abstract

The reaction temperature plays a key role in observing biochemical reactions through a microscope. In conventional methods, the actual local temperature of the observed area is different from the measured local temperature because the heater and the temperature sensor are far apart. The electrical resistance of indium tin oxide, a transparent electrode, changes with its temperature. Based on this property, we developed a temperature control system for the viewing area of a microscope. In this system, we heated the transparent electrode by Joule heating, and temperature measurement is conducted on the same electrode in a time-sharing manner. Then, we applied this system to temperature cycles for a reverse transcription-polymerase chain reaction in emulsions. Successful DNA amplification was confirmed by observing the fluorescence of FAM, whose quenching was terminated via oligonucleotide cleavage by DNA amplification in the emulsions.

Keywords: Indium tin oxide (ITO) electrode, temperature sensor, temperature control, polymerase chain reaction (PCR).

1. Introduction

The development of microelectromechanical systems (MEMSs) and susceptible microscope systems has enabled the analysis of interactions between biological molecules and functions at the single-molecule level under fluorescence microscopes [1−5]. However, while biochemical reactions in MEMS appear in the viewing area of a microscope, it is difficult to control the temperature of the reaction field because both the temperature sensor and heater are usually far from the reaction field. Moreover, even in the reaction field in a microchannel, the temperature of the reaction liquid to be injected and the set temperature in the transparent chamber differ due to the intense excitation light of the microscope [6−8].

To solve this problem, we developed a temperature control method based on a transparent heater–sensor electrode, an electrode applied to both heat generation and temperature sensing. First, we used Al-doped zinc oxide (AZO) [9, 10] and indium tin oxide (ITO) [11, 12] thin-film-deposition substrates to build transparent heater–sensor electrodes, and we investigated their temperature characteristics. We measured the resistance of the electrodes with rising temperature and then determined the relationship between their temperature and electrical resistance. Findings suggested that ITO is more suitable for this purpose, therefore we developed the proposed system using the ITO electrode. Next, we designed an electrical circuit both for temperature sensing and heating, and also developed a temperature control program for the ITO heater–sensor electrode and optimized the control parameters. Finally, we applied this system to reverse transcription (RT) polymerase chain reaction (PCR) [13, 14] in order to demonstrate that the temperature can be precisely controlled. We successfully performed DNA amplification via RT-PCR in emulsions [15, 16] on the ITO electrode, which confirmed that the temperature was cyclically controlled between 94 and 60°C.

2. Experimental setup

2.1 Chemicals

Primers were ordered from Integrated DNA Technologies (IDT; Coralville, IA, US). Abil EM 90 as an emulsifier was purchased from Evonik Japan (Tokyo, Japan). The bacteriophage MS2 (NBRC 102619) and *Escherichia coli* (Migula 1895) Castellani and Chalmers 1919 (host cells for MS2; NBRC 13965) were obtained from the National Institute of Technology and Evaluation (Tokyo, Japan). All reagents were of biotechnology grade and purchased from Sigma-Aldrich (St. Louis, MO, US), Fujifilm Wako Pure Chemical (Osaka, Japan), and Nacalai Tesque (Kyoto, Japan).

2.2 Fabrication and temperature characteristics of AZO and indium tin oxide electrodes

Glass substrates with AZO or ITO vapor deposited film were purchased from Geomatec Co. Ltd. (Yokohama, Kanagawa, Japan) and cut into 20 × 32 mm pieces. The AZO substrate (product number 0071) had a resistance value of ≤ 40 Ω/sq, film thickness of 150 nm, and transmittance of ≥ 88% with a wavelength of 550 nm (public data of Geomatec Co. Ltd.). The ITO substrate (product number 1002) had a resistance value of 10 ± 2 Ω/sq, a film thickness of 150 ± 20 nm, and transmittance of ≥ 80% with a wavelength of 400 to 700 nm (public data of Geomatec Co. Ltd.). Aluminum foil was placed on the surface of the AZO/ITO substrate with silver paste (Kaken Tech Co. Ltd., Katano, Osaka, Japan) so that the distance between the electrode and the length of the electrode surface was 10 × 10 mm (reaction area). The aluminum foil was attached to conducting wire with silver paste to prepare AZO and ITO electrodes (Fig. 1). We constructed a bridge circuit to measure changes in electrical resistance. The deviation from the equilibrium of the bridge circuit was amplified with an instrumentation amplifier (LT1167, Analog Devices, Norwood, MA, US), and the amplified voltage value was recorded on an Arduino Due microcontroller board (Fig. 2). Each electrode and a K-type (chromel alumel) thermocouple temperature sensor (MAX31855, Switch Science, Tokyo, Japan) were placed in a constant-temperature oven (ON-300SB, As One, Osaka, Japan). The thermocouple measured the surface temperature of the electrode, and the measured temperature was transmitted to a PC through an Arduino Uno microcontroller board and then logged. The Arduino Due recorded the electrical resistance of the electrode surface while we gradually increased the temperature of the constant-temperature oven from room temperature to 100°C.

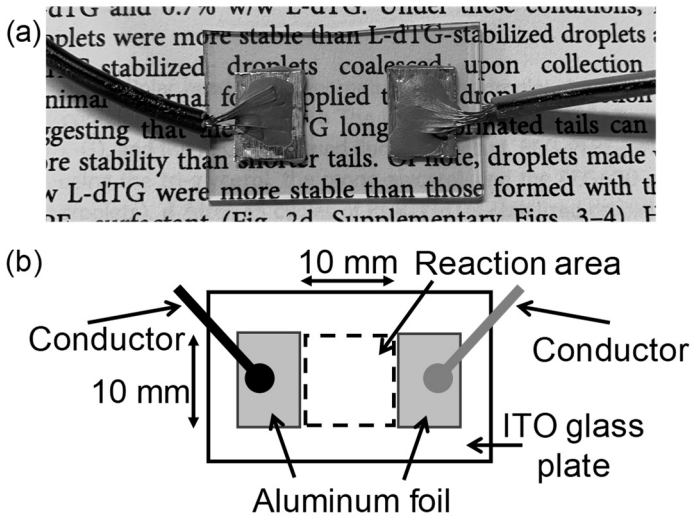

Fig. 1. Prepared indium tin oxide electrode. (a) Photograph of the electrode, (B) schematic diagram of the electrode. The Al-doped zinc oxide electrode was prepared in the same manner (photograph and schematic diagram not shown).

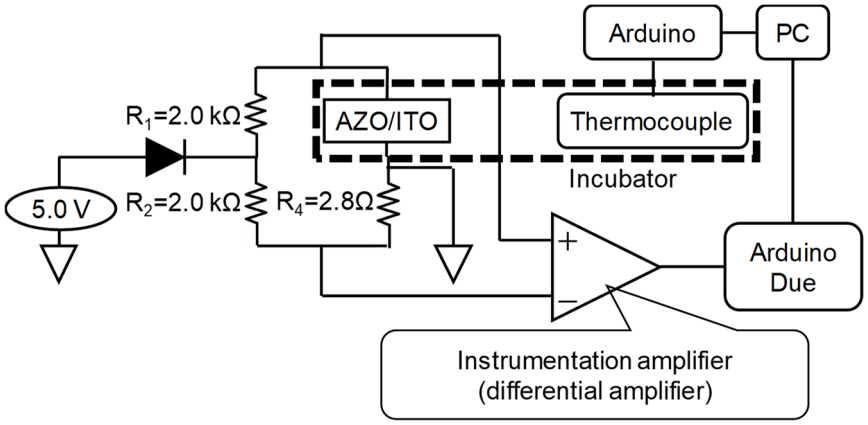

Fig. 2. Diagram of the electrical circuit for measuring the temperature and resistance of the Al-doped zinc oxide and indium tin oxide electrodes.

2.3 Temperature control by proportional–integral control of indium tin oxide electrode

Details on the temperature characteristics of the AZO and ITO electrodes are shown in the Results and Discussion. The ITO electrode was superior to the AZO electrode. Therefore, we developed a temperature control device for the ITO electrode. First, an electric circuit for temperature control was designed to control the power applied to heat the ITO electrode (Fig. 3). The applied power was controlled via pulse-width modulation (PWM), based on changing the duty ratio of pulses. In this system, the transparent electrode by Joule heating (about 300 ms), and temperature measurement (about 50 ms) was conducted on the same electrode in a time-sharing manner. Next, proportional–integral (PI) control was implemented as the temperature control method of the ITO electrode. The error between the target and measured temperatures in the PI control system was obtained. According to the PI control method, feedback heat power is proportional to the error and its integrated value. We determined the coefficients (proportional and integral) affecting system behavior through trial and error.

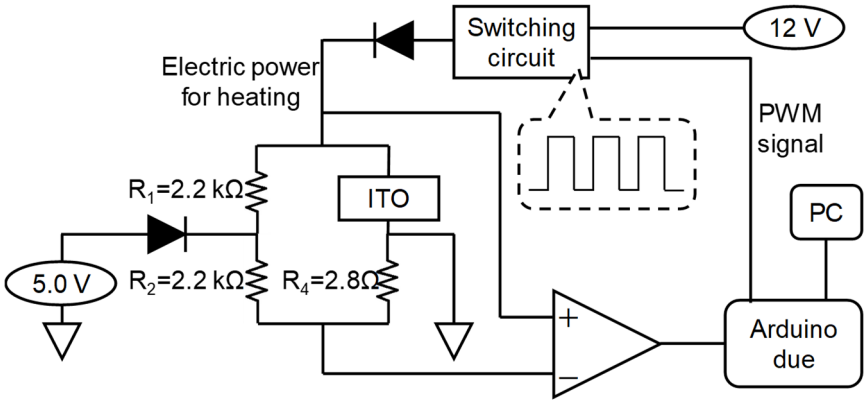

Fig. 3. Diagram of the electrical circuit for the heating control of the indium tin oxide electrode via PWM.

2.4 Step response and proportional–integral–derivative control of indium tin oxide electrode

Derivative control was added to suppress temperature oscillation and achieve quick convergence to the target. A proportional–integral–derivative (PID) control system is a standard method, but if we input a stepwise target temperature, the derivative of the error becomes infinite. Since the target temperature would change stepwise during the PCR temperature cycle, PI-D control, which would use the derivative of the temperature instead of the error, was adopted. To optimize the coefficients for PI-D control, we developed a simulation system with a "control Matlab" module in Python. A constant power (1.33 W) was applied to the ITO electrode, and we measured the step response of the temperature according to the resistance change in the ITO electrode. Based on the result of the step response, the dead time, delay time, and saturation temperature of the controlled object

(ITO electrode) were determined. The coefficients for PI-D control were optimized by the developed simulator using these parameters.

2.5 Thermal control according to PCR program of indium tin oxide electrode

To confirm whether we could modify the reaction by controlling the temperature of the ITO electrode, we created a control program for one-step RT-PCR. This reaction was a continuous RT reaction and PCR. The output of the instrumentation amplifier, which reflected the temperature, was acquired via the Arduino Due and converted into temperature according to the calibration curve (see Fig. 4 (b)). The following conditions were set for the one-step RT-PCR temperature cycle control program: (1) RT reaction at 45°C for 600 s; (2) thermal denaturation at 95°C for 120 s; and (3) 40 thermal cycles at 95°C for 10 s and 60°C for 30 s. This reaction was performed by placing the ITO electrode on the microscope stage. An air-cooling fan (Panaflo FBA06T12M, Panasonic, Kadoma, Osaka, Japan) was installed above the ITO glass substrate to promote cooling and shorten the PCR time. The Arduino Due controlled the fan to operate until the surface temperature of the ITO substrate reached 65°C during the cooling stage of the PCR program.

2.6 One-step emulsion RT-PCR amplification by fluorescent probe method on indium tin oxide electrode and observation of emulsions

RT-PCR was carried out both to demonstrate this system can be applied to bacteriophage MS2 as the model of RNA viruses (influenza virus, COVID-19, hog cholera, etc.) detection and to confirm that multi-step temperature control is possible, including control of 45°C in the reverse transcription reaction. RT-PCR was attempted to demonstrate precise control of temperature, however, it was difficult both to recover RT-PCR products from the device and to analyze the amplified DNA by agarose gel electrophoresis. Therefore, we applied emulsion RT-PCR amplification to the transparent electrode system. Concentrated bacteriophage (MS2; 1.1×10^7 plaque-forming units [PFU]) was used as the RT-PCR template. The MS2 genome is a single-stranded RNA molecule of 3569 bases. We used the following amplification primers for gene amplification: MS2-3F: 5'-CGT TCA CAG GCT TAC AAA GTA ACC T-3' and MS2-3R: 5'-CCA ACA GTC TGG GTT GCC AC-3' (16). The 106 bp of DNA fragment was amplified by the primer set. Fluorescein amidite (FAM)–labeled probes were used to detect MS2 (AGA ATC GCA AAT ACA CCA ATC AAA GTC GAG GT-ZEN/IBFQ) [17]. The RT reaction was performed with the reverse primer (MS2-3R), and IDT synthesized the oligonucleotides. Then, 20 μL of the RT-PCR reaction solution (MyGo Probe 1-Step No ROX, IT-IS Life Science Ltd., Dublin, Ireland) was prepared as the aqueous phase. The PCR reaction solution was added dropwise to 100 μL of an oil phase that included mineral oil (Nuclease and Protease tested, 23306-84, Nacalai Tesque), 2% (v/v) Abil EM90, and 0.05% (v/v) Triton X-100, and the mixture was stirred to form emulsions. A micro stirring rod (5 × φ2 mm, 1-3252-02, As One), screw tube bottle (9-852-03, As One), and magnetic stirrer (HSD-4, As One) set at about 300 rpm was used in stirring. Next, 20 μL of the prepared emulsion was dropped onto the reaction area on the ITO electrode, which was then covered with a cover glass. The temperature control program of the ITO electrode was executed, followed by observation with a fluorescence microscope (Eclipse TE2000-U, Nikon, Tokyo, Japan) at objective lens magnifications of 40× and 100×. This one-step emulsion RT-PCR involves the fluorescent probe method, in which droplets in the emulsion fluorescence when the target DNA fragment in them are amplified. Bright-field microscope images confirmed the position and shape of droplets in the emulsions with white LED light. The fluorescence of FAM, whose quenching was terminated via oligonucleotide cleavage by DNA amplification in the emulsions, was confirmed using the fluorescence microscope with a blue-light excitation filter (490 nm).

3. Results and discussion

3.1 Temperature characteristics of AZO and ITO electrodes

Fig. 4 shows the relation between the electrode surface temperature and the output of the instrumentation amplifier for the shift from the equilibrium of the bridge, acquired through the 12-bit AD converter in Arduino Due. The temperature was measured with the thermocouple connected to the Arduino Uno while the oven temperature gradually increased. As the surface temperatures of the AZO and ITO electrodes increased, the

output voltage of the instrumentation amplifier also increased. As for the temperature characteristics of the two electrodes, the ITO electrode showed a smaller voltage change than the AZO electrode but had higher linearity. Therefore, the ITO electrode was a better temperature sensor, and it was used in the subsequent experiments.

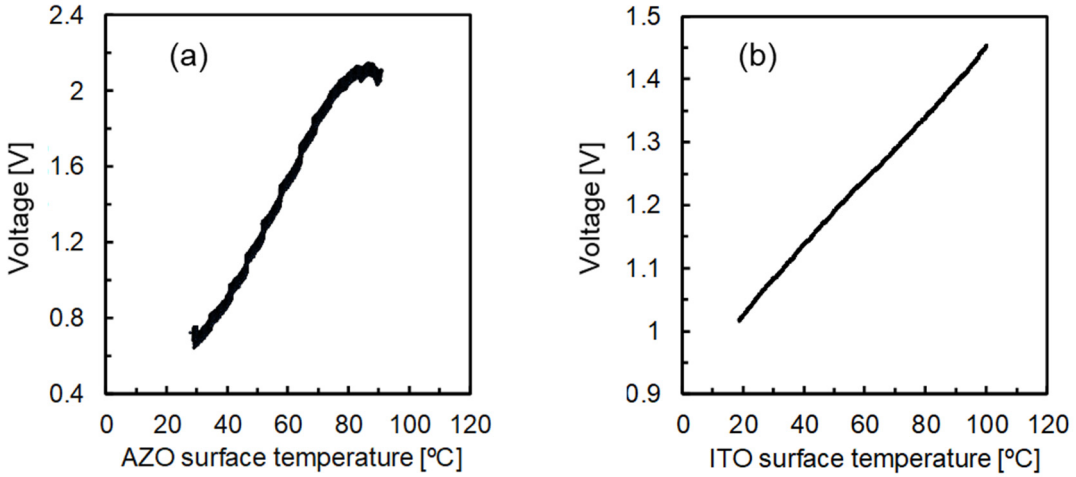

Fig. 4. Relation between the electrode surface temperature and the output from the instrumentation amplifier for the shift from the equilibrium of the bridge. (a) AZO and (b) ITO

3.2 Temperature control by PI control of ITO electrode

Fig. 5 shows the results for proportional (P) control and PI control with the target value of 70°C for the ITO electrode. Under PI control, the deviation from the target temperature 27 s after the start of control was within 1°C, and the target temperature was reached after 41 s. However, the target temperature was not reached under P control.

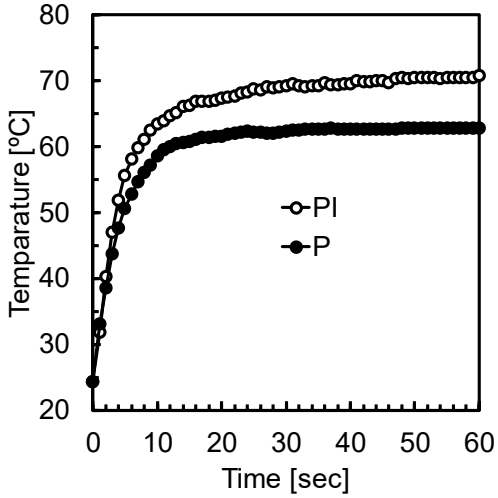

Fig. 5. Results of P and PI control with the target value of 70°C for the indium tin oxide electrode.

3.3 Step response by voltage application to ITO electrode

Constant power (1.33 W) was applied to the ITO electrode to obtain a step response, and we measured the time change of the shift of the bridge from the equilibrium, which reflected the temperature. Fig. 6 shows the temperature deviation from room temperature. Our analysis of the step responses showed the following parameters of the controlled objects: dead time of 1.198 s, a delay time of 85.94 s, and saturation temperature from room temperature of 57.45°C. We optimized the PI-D gain using these parameters.

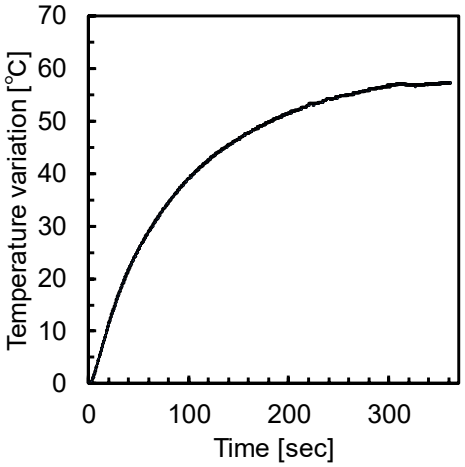

Fig. 6. Temperature deviations of the indium tin oxide electrode from room temperature.

3.4 Thermal control according to PCR program of ITO electrode

The one-step RT-PCR program was executed under ITO temperature control, and temperature changes over time were measured. Findings confirmed that we could perform temperature control according to the PCR program on the ITO electrode. Implementation of the entire PCR program consumed about 70 min. Nonetheless, with the air-cooling fan placed above the ITO electrode, we controlled the temperature from 95°C to 65°C and measured the temperature change over time (Fig. 7 (a)). By installing the fan, we successfully reduced the time required for the PCR program. The total time was about 58 min, which indicated a reduction of 12 min (Fig. 7 (b)). Hence, a Peltier element, a general-purpose cooling device, is no longer necessary.

3.5 One-step emulsion RT-PCR on ITO electrode

Before performing one-step emulsion on ITO electrode, one-step RT-PCR from bacteriophage MS2 in PCR tube was confirmed. The reaction solution followed the protocol in MyGo Probe 1-Step No ROX, including bacteriophage MS2 (1.1×10^7 PFU), MS2-3F, MS2-3R and FAM–labeled probe. The reaction products were confirmed by 1% agarose gel electrophoresis. (Fig. 8). As a result, an amplified DNA fragment was identified at approximately 0.1 kbp, which was the size of the designed DNA fragment.

The bacteriophage MS2 (1.1×10^7 PFU) as the template was prepared for RT-PCR in the dispersive phase of the emulsion. The solution was dropped onto the ITO electrode, and the one-step emulsion RT-PCR program was executed. The aqueous droplets in the emulsion were observed through the bright-field mode of the microscope. In contrast, droplets containing the amplified DNA fragments by RT-PCR were observed via the fluorescence mode of the microscope (Fig. 9). The fluorescence of the emulsion was due to the fluorescence of FAM cleaved from the probe. It shows the result of specific amplification of the DNA fragment recognized by both the primer set and the fluorescent probe. According to the prepared bacteriophage MS2 concentration, the average number of phages in the droplets would be estimated as 30, when the diameter of the droplets is assumed to be 25 μm, which is a typical diameter of the fluorescent droplets as shown in Fig.9 (c) and (d). Under this experimental condition, almost all the droplets contained some RNA template, and successful amplification was confirmed in droplets greater than 25 μm in diameter. This demonstrates that the number of RNA phages in each droplet was sufficient for RT-PCR amplification under our experimental condition. However, when the droplets were 12 μm in diameter, some droplets show amplification and the others show no amplification of template RNA (Fig. 9 (e) and (f)). When the diameter of the droplets was assumed to be 12 μm, the average number of template RNA in the droplets could be evaluated as 0.5. According to Poisson distribution, about 60% of droplets would contain no RNA template, therefore, there was no significant difference between this expected value and the number of fluorescent droplets. By using the transparent heater–sensor electrode, we developed the temperature control device that can be applied to both heat generation and temperature detection.

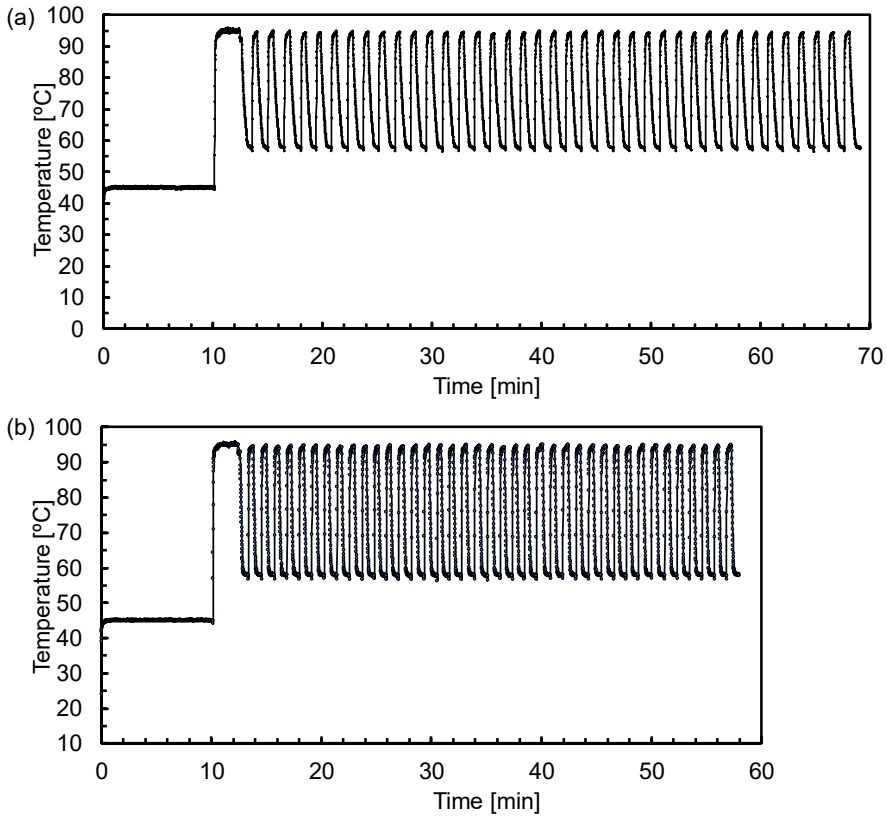

Fig. 7. Diagram of the temperature changes of the indium tin oxide electrode via the one-step RT-PCR program. (a) Without the air-cooling fan, (b) with the air-cooling fan.

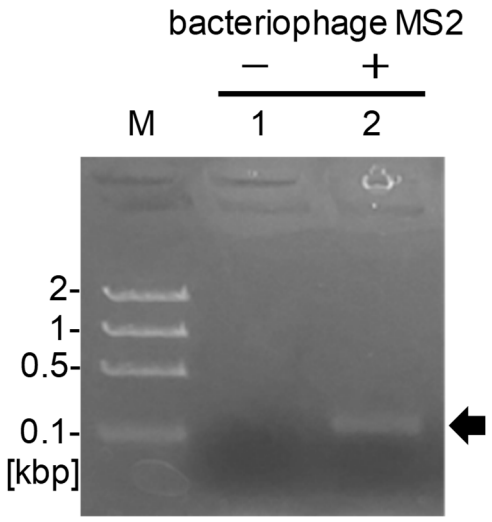

Fig. 8. Results of RT-PCR with bacteriophage MS2 as a template in bulk. M: DNA molecular weight markers (Gene Ladder Fast 1 (0.1-2 kbp), NIPPON GENE CO., LTD., Tokyo, Japan), lane 1: without bacteriophage MS2 for a template, lane 2: with bacteriophage MS2 (1.1×10^7 PFU in reaction), arrow: amplified DNA fragments.

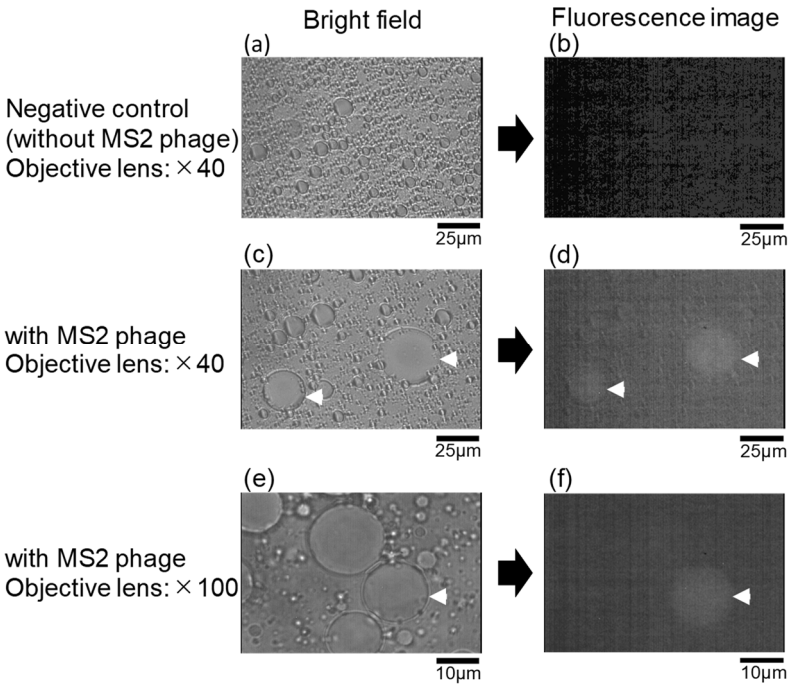

Fig. 9. Results of bacteriophage MS2 detection via emulsion RT-PCR on the indium tin oxide electrode. (a) and (b) Negative control (without MS2 phage). (c) and (d) 40× objective lens. (e) and (f) 100× objective lens. (a), (c) and (e): photos of bright field. (b), (d) and (f): photos of fluorescence image. The emulsions indicated by the white arrowheads emitted positive fluorescence signals in (d) and (f). Three experiments were performed with similar results.

4. Conclusion

Using a bridge circuit and an instrumentation amplifier, the device was created to measure the resistance of the transparent electrode and determine the temperature. The temperature-voltage characteristics were found to be more linear and superior for the ITO electrode compared to the AZO electrode. The temperature of the ITO electrode could be controlled by adjusting the heating power through PI-D control. The temperature of the ITO electrode was successfully controlled to follow a temperature cycle suitable for PCR. One-step emulsion RT-PCR using the probe method was then performed by controlling the temperature of the ITO electrode, and DNA amplification was confirmed.

Acknowledgment

This work was partly supported by JSPS KAKENHI Grant-in-Aid for Scientific Research (C) (21K04074) (S.K.) and the research fund of Amano Institute of Technology (M.O.).

References

[1] Shinde, P., Mohan, L., Kumar, A., Dey, K., Maddi, A., Patananan, A. N., Tseng, F. G., Chang, H. Y., Nagai, M., and Santra, T. S., Current trends of microfluidic single-cell technologies, *Int. J. Mol. Sci*, Vol. 19 (10), 3143, 2018.
[2] Saper, G., and Hess, H., Synthetic systems powered by biological molecular motors, *Chem. Rev.*, Vol. 120 (1), pp. 288-309, 2019.
[3] Ghazali, F. A. M., Hasan, M. N., Rehman, T., Nafea, M., Ali, M. S. M., and Takahata, K., MEMS actuators for biomedical applications: a review, *J. Micromech. Microeng.*, Vol. 30, 073001, 2020.
[4] Zhou, G., Lim, Z.H., Qi, Y., and Zhou, G., Single-pixel MEMS imaging systems, *Micromachines*, Vol. 11 (2), 219, 2020.

[5] Takahashi, S., Oshige, M., and Katsura, S., DNA Manipulation and Single-Molecule Imaging, *Molecules*, Vol. 26 (4), 1050, 2021.
[6] Ghodke, H., Ho, H., and van Oijen, A. M.: Single-molecule live-cell imaging of bacterial DNA repair and damage tolerance, *Biochem. Soc. Trans.*, Vol. 46 (1), pp. 23−35, 2018.
[7] Takahashi, S., Motooka, S., Kawasaki, S., Kurita, H., Mizuno, T., Matsuura, S. I., Hanaoka, F., Mizuno, A., Oshige, M., Katsura, S., Direct single-molecule observations of DNA unwinding by SV40 large tumor antigen under a negative DNA supercoil state, *J. Biomol. Struct. Dyn.*, Vol. 36 (1), pp. 32−44, 2018.
[8] Swaminathan, J., Boulgakov, A. A., Hernandez, E. T., Bardo, A. M., Bachman, J. L., Marotta, J., Johnson, A. M., Anslyn, E. V., and Marcotte, E. M., Highly parallel single-molecule identification of proteins in zeptomole-scale mixtures, *Nat. Biotechnol.*, Vol. 36 (11), pp. 1076−1082, 2018.
[9] Badgujar, A. C., Yadav, B. S., Jha, G. K., and Dhage, S. R., Room Temperature sputtered aluminum-doped ZnO thin film transparent electrode for application in solar cells and for low-band-gap optoelectronic devices, *ACS Omega*, Vol. 7 (16), pp. 14203−14210, 2022.
[10] Nath, B., Ramamurthy, P. C., Hegde, G., and Roy Mahapatra, D., Role of electrodes on perovskite solar cells performance: A review, *ISSS J. Micro and Smart Systems*, Vol. 11, pp. 61–79, 2022.
[11] Fernández, S., González, J. P., Grandal, J., Braña, A. F., Gómez-Mancebo, M. B., and Gandía, J. J., Roles of Low temperature sputtered indium tin oxide for solar photovoltaic technology, *Materials*, Vol. 14 (24), 7758, 2021.
[12] Kuzovlev, A. N., Evseev, A. K., Goroncharovskaya, I. V., Shabanov, A. K., and Petrikov, S. S., Optically transparent electrodes to study living cells: A mini review, Biotechnol. Bioeng., Vol. 118 (7), pp. 2393−2400, 2021.
[13] Clementi, M., Menzo, S., Bagnarelli, P., Manzin, A., Valenza, A., and Varaldo, P. E., Quantitative PCR and RT-PCR in virology, *PCR Methods Appl.*, Vol. 2 (3), pp. 191−196, 1993.
[14] Chen, P., Du, Y., Xu, Y.Z., Liu, Z., and Yan, K., Review: Bioaerosol collection, *Int. J. Plasma Environ. Sci. Technol.*, Vol.11 (1), pp. 52−55, 2017.
[15] Nakano, M., Komatsu, J., Matsuura, S., Takashima, K., Katsura, S., and Mizuno, A., Single-molecule PCR using water-in-oil emulsion, *J. Biotechnol.*, Vol. 102 (2), pp.117−124, 2003.
[16] Nakano, M., Nakai, N., Kurita, H., Komatsu, J., Takashima, K., Katsura, S., and Mizuno, A., Single-molecule reverse transcription polymerase chain reaction using water-in-oil emulsion, *J. Biosci. Bioeng.*, Vol. 99 (3), pp. 293−295, 2005.
[17] O'Connell, K. P., Bucher, J. R., Anderson, P. E., Cao, C. J., Khan, A. S., Gostomski, M. V., and Valdes, J. J., Real-time fluorogenic reverse transcription-PCR assays for detection of bacteriophage MS2, *Appl. Environ. Microbiol.*, Vol. 72 (1), pp. 478−483, 2006.